International Journal of Chemical Kinetics

WILEY

RESEARCH ARTICLE OPEN ACCESS

Ab Initio Study of the Gas- and Liquid-Phase Hydrogen Abstraction From Dimethyl-, Diethyl-, and Ethyl–Methyl Carbonates by Ḣ and Ċ H_3 and Subsequent Reactions

Marwa Saab[1] | Yann Fenard[1] | Guillaume Vanhove[1] | Malte Döntgen[2] | K. Alexander Heufer[2]

[1]Univ. Lille, CNRS, UMR 8522 – PC2A, Physicochimie des Processus de Combustion et de l'Atmosphère, Lille, France | [2]Chair of High Pressure Gas Dynamics, Shock Wave Laboratory, RWTH Aachen University, Aachen, Germany

Correspondence: Malte Döntgen (doentgen@hgd.rwth-aachen.de)

Received: 18 December 2024 | **Revised:** 17 July 2025 | **Accepted:** 24 July 2025

Funding: This study was supported by ANR SFRI (21-SFRI-0005) GRAEL program of the University of Lille, The French National Research Agency (ANR) through the PIA (Programme d'Investissement d'Avenir) under contract "ANR-11-LABX-0005–01", the "European Funds for Regional Economical Development" (FEDER), the Deutsche Forschungsgemeinschaft (DFG, German Research Foundation) – 535189852.

Keywords: ab initio | diethyl carbonate | dimethyl carbonate | ethyl–methyl carbonate | H-abstraction

ABSTRACT

Dimethyl-, diethyl, and ethyl–methyl carbonate are important components of lithium batteries. They are used as solvents and comprise the medium through which the lithium ions move between the anode and the cathode during charge and discharge. However, these species are susceptible to decomposition if thermal runaway occurs, forming flammable gases inside the battery, and eventually leading to mechanical failure and ignition with the surrounding air. These events have been reported and are extremely hazardous. To avoid these incidents, it is important to understand the reactivity of carbonates by building chemical kinetic mechanisms based on experimental testing and theoretical calculations. These models are also important when using these species in combustion as additives or replacements to fossil fuels. Because of their high oxygen content, researchers believe that including carbonates in combustion processes would decrease soot and particulate matter emissions. Existing models typically use estimated reaction rate parameters; thus, more accurate rate parameters would benefit existing and new models. In this study, the rate coefficients of H-atom abstraction reactions by Ḣ and Ċ H_3, β-scission, isomerization, and internal radical migration reactions are computed from CCSD(T)/aug-cc-pV(D+T)Z//B3LYP-D3BJ/def2-TZVP calculations. Additionally, solvation effects have been investigated to allow for comparison between liquid and gas phase kinetics. Consistent with the literature, H-atom abstraction by Ḣ is found to be faster than that by Ċ H_3. At the low-temperature end of the investigated range (300 K), available literature rate coefficients and the present rate coefficients are deviating up to three orders of magnitude. Notably, uncertainties in the imaginary frequency computation are found to contribute most to deviations between the present calculations and combined theoretical and experimental literature data for DMC + Ḣ. For the unimolecular reactions of the fuel radicals, β-scission is found to dominate radical consumption and differs from previous analogy-based rates by up to about one order of magnitude. Solvation effects are found to be pronounced for diethyl and ethyl–methyl carbonate, with up to two orders of magnitude faster isomerization in the liquid phase compared to the gas phase. The presented rate coefficients will aid future detailed chemical kinetic modeling.

1 | Introduction

The demand for finding a clean source of energy has been increasing in tandem with the massive climate change. Knowing that carbon dioxide emissions are a significant key in this problem, researchers have been making a lot of effort to find an efficient alternative to burning fossil fuels [1].

Pure or hybrid electric vehicles are now dominating the market as one of the best in terms of decreasing pollutant emissions [2]. A significant number of these vehicles operate on rechargeable lithium-ion batteries [3]. However, even at normal operating conditions [4], a thermal runaway hazard may occur according to the activity and combustibility of the traditional battery components [5]. Carbonate esters are a dominant constituent in the battery, as they comprise the medium through which the lithium ions move between electrodes during the charge and discharge cycles [6], but they are flammable substances. Accordingly, it is important to understand the reactivity of these carbonates to be able to inhibit ignition, and thus increase the durability and safety of these batteries.

Carbonate esters can also be employed as potential biofuel additives or replacements to petroleum-derived diesel fuels. Since these species are oxygenated, it is likely that this would decrease the soot and particulate matter (PM) emissions [7–9].

Looking at the variety of applications for these carbonate esters, diverse studies have been performed. In this context, we will focus on three different carbonates: dimethyl-, diethyl-, and ethyl–methyl carbonates (DMC, DEC, and EMC, respectively).

The combustion of DMC was studied by Sinha and Thomson [10] using a counterflow diffusion flame in which the species concentrations were measured, followed by the study of Glaude et al. [11], using the same experiments to build a kinetic mechanism for DMC of which the rates targeted in this study were all estimated from different literature mechanisms. Bardin et al. [12] measured laminar burning velocities of DMC with air using the heat flux method, where the flame was stabilized on a perforated plate burner at atmospheric pressure. Furthermore, Henriksen et al. [13] used a 20-L explosion sphere to determine the laminar burning velocity of DMC and propane at pressure of 100 kPa and temperature of 300 K. Hu et al. [14] and Alexandrino et al. [15] studied the ignition of DMC using a rapid compression machine and a shock tube, whereas Atherley et al. [16] used a shock tube also for spectroscopic measurements to measure time histories of CO and H_2O. Most importantly for the present work, Peukert et al. [17] studied DMC pyrolysis experimentally with complementary ab initio calculations, providing rate coefficients for H-atom abstraction by Ḣ, among others.

The ignition delay times of DEC were measured using a rapid compression machine and a shock tube by Nakamura et al. [18] in order to help build a kinetic mechanism where rate constants of H-abstraction reactions were all based on analogies with ethyl esters or alkanes. To build a kinetic model for DEC high-temperature pyrolysis and combustion, Sun et al. [19] recorded the mole fractions of species using gas chromatography during pyrolysis of DEC in a flow reactor. The authors used analogies to ethyl esters to model the rates of H-atom abstraction reactions and the subsequent reactions. Shahla et al. [20] measured stable species using a jet stirred reactor to validate the model from Nakamura et al. [18]. They also measured the burning velocities of DEC/air mixtures. AlAbbad et al. [21] investigated the initial pyrolytic steps experimentally and theoretically, and their results show good agreement with the values from Notario et al. [22] at low temperatures. Sela et al. [23] extended the temperature range of directly measured rate constant data for the unimolecular decomposition of DEC, their results show a good agreement with some reported literature data [24, 25], and a significant deviation from others [26].

Few pyrolysis studies have been performed on EMC. Using a reaction vessel, Taylor [27], Cross et al. [24], and Gordon and Norris [26] measured decomposition rates of EMC around 600 K. Theoretical decomposition rates have been computed by Notario et al. [22], Añez et al. [28], and Chuchani et al. [29]. Takahashi et al. [30] studied the reactivity of DMC, DEC, and EMC in the gas phase using a weak flame in a micro flow reactor, and then in a complementary study [31], they developed a chemical kinetic mechanism for EMC based on the mechanism of Nakamura et al. [18] for DEC. Recently, Grégoire et al. [32] used shock tube spectroscopic CO measurements to study the pyrolysis of the three title carbonates.

In the present study, we provide calculated rate coefficients for the H-abstraction reactions by Ḣ and Ċ H_3 and the subsequent reactions for DMC, DEC, and EMC radicals, as it is clear now that all the existing mechanisms are largely based on estimated rate parameters for these reactions. Moreover, we considered both gas and liquid phases to take into consideration the effects of solvation on the reactivity of these carbonates, which has not been investigated until now. Barnes et al. [6] performed ab initio characterization of the solvation properties of DMC, but they did not target the aforementioned reactions. The importance of these reactions lies in the fact that they take place in pyrolysis and oxidation, which means that their rates are valuable for all chemical kinetic mechanisms.

2 | Computational Methods

2.1 | Gas Phase

The Gaussian 16 software, Revision C.01 [33], was used for all electronic structure calculations in this work. Geometries and vibrational harmonic frequencies are computed at the B3LYP-D3BJ/def2-TZVP level of theory throughout the study. This level of theory is a well-established method for decades, and computationally not expensive, so it is sufficient to obtain accurate results with reasonable computational efforts.

The geometries from this method are used to calculate single-point energies (SPEs) at the CCSD(T) level of theory with augmented double- and triple-zeta basis functions (aug-cc-pV(T+D)Z). The complete basis set (CBS) extrapolation is done following the approach described in [34]. The accuracy of this method for hydrogen abstraction barriers has been assessed to

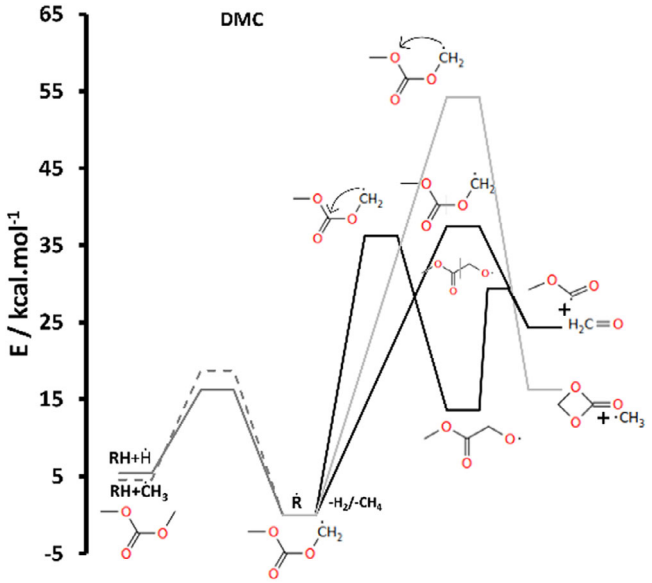

FIGURE 1 | Potential energy surface of DEC H-abstraction by Ḣ and Ċ H_3, radical isomerization, internal radical migration, and β-scission for two radicals. The energy of DEC Ṙ 1 is set to zero and energetic differences due to different stoichiometric formulas are accounted for by subtracting the energies of H_2 and CH_4. The energies are zero-point corrected at 0 K.

be ±0.57 kcal/mol [35]. T1-diagnostics are used to check the resilience of the single-reference approach and were all found to be well below 0.044 [36].

Relaxed 1D rotor scans with a 30° increment were performed using the same method as described above to establish the minimum energy conformer. When these scans declared a new minimum, then the corresponding structure was used for new subsequent 1D scans. This loop prevailed until the lowest energy conformer was found.

These minimum energy conformers, the 1D hindered rotors potential energy profiles, and the SPEs were then used to calculate the rate constants. Thus, we assume that the structure with minimal energy, in combination with the 1D scans, accounts for the relevant conformational space. While we acknowledge that this is not always assured, we have confidence that this method is adequate for the compounds investigated here.

The conventional transition state theory (cTST) and the zero-curvature Eckart approach for tunneling are used to calculate the reaction rate constants for hydrogen abstraction. Because of the high energy barriers and imaginary frequencies, variational effects are expected to be of minor importance.

The rate constants are calculated for temperatures from 500 to 2000 K for combustion applications and are provided in the Supporting Information (SI). Regarding the thermal runaway of a battery, it occurs over time, starting from room temperature. Accordingly, another set of calculations was also done at lower temperatures, from 300 to 700 K for both the gas phase and the liquid phase for a direct comparison in the present study.

Temperature- and pressure-dependent rate constants for the unimolecular β-scission, internal radical migration, and isomerization are calculated via the Master Equation (ME) using the MESS software package [37]. Collisional relaxation has been modeled using the Lennard-Jones (LJ) collision frequency model [38] in combination with the single-exponential down model. For the collision frequency model, the LJ parameters σ = 4.93, 5.23, and 5.48 Å and ε = 693.2, 786.7, and 877.7 K have been used for DMC, EMC, and DEC, respectively. These parameters have been obtained using the adopted 1D-min approach as detailed in [39]. For the bath gas nitrogen, the parameters σ = 3.7 Å and ε = 85.2 K have been obtained from [40]. The single-exponential down model uses an average energy deactivation of $\langle E_{\text{down}} \rangle = 200\ \text{cm}^{-1} \cdot (T/300\text{K})^{0.85}$.

2.2 | Solvation

To compute the liquid-phase rate parameters, the optimized gas-phase structures were re-optimized at the same level of theory using the polarizable continuum model (PCM) of the Gaussian software package. The rotor scans, however, have not been recalculated, as these are expected to change only marginally. Re-using the potential energies of the gas-phase hindered rotor scans is based on the assumption that the relative energies along the torsional modes are not strongly influenced by the PCM model. Thus, we modeled the liquid phase hindered rotations based on the gas-phase hindered rotor potential energy profiles. The SPEs have been recalculated using the previously used level of theory, but with the PCM.

The permittivity used for the three solvents is ε = 19 as verified by Self et al. [41] for lithium ion battery electrolyte environments. Pressure-dependent rate coefficients have been calculated using the MESS software package, yet only the high-pressure limits are used in the following discussion for clarity.

Note that for the SPEs with PCM, the standard state is 298 K and 1 mol/L, in contrast to the ideal gas phase standard state at 1 atm. By default, Gaussian provides results at the ideal gas phase standard state. This necessitates correcting the free enthalpy by R•T•ln(1 mol/L/$\rho^{(g)}$(T)) for each species and transition state [42]. While this correction cancels out for unimolecular reactions, it does affect bimolecular reactions, such as H-atom abstractions. In the transition state theory formulation, the free enthalpy correction translates to a prefactor of 0.0820528•T/K for the rate coefficient expression. This is included as a correction to the A-factor and the temperature exponent by A•0.0820528 and n+1, respectively.

3 | Results and Discussion

3.1 | Potential Energy Surfaces

The potential energy surfaces (PESs) for DMC and DEC are represented in Figures 1 and 2, respectively (cf. SI for EMC PES). The H-atom abstraction reactions and unimolecular fuel radical reactions are shown on the plot for a consolidated view of the chemistry. This is done by correcting the hydrogen abstraction reaction energies by the products of the abstracting radicals, i.e., H_2 or CH_4. This representation immediately reveals that so-called hot β-scission [43] is not relevant in the case of dialkyl carbonates,

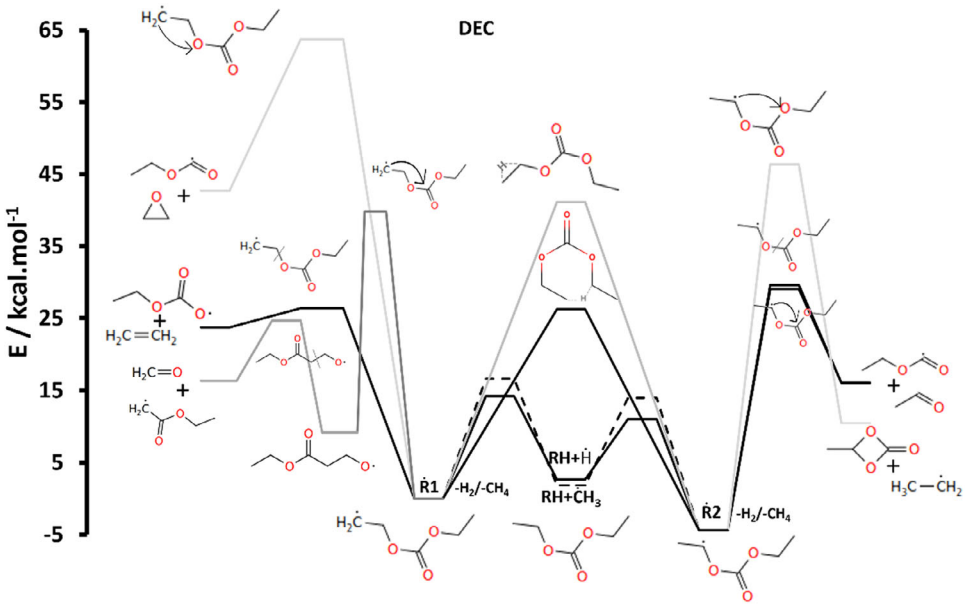

FIGURE 2 | Potential energy surface of DMC H-abstraction by Ḣ and Ċ H_3, radical isomerization, internal radical migration, and β-scission. The energy of DMC Ṙ is set to zero and energetic differences due to different stoichiometric formulas are accounted for by subtracting the energies of H_2 or CH_4. The energies are zero-point corrected at 0 K.

at least not for the considered abstracting radicals. The energies of the relevant stationary points on the PES are provided in Table 1.

In the three PESs there are three different pathways for each radical. The PES of DMC is the simplest as it produces only one radical, followed by DEC, which produces two radicals, and lastly EMC, which produces three different radicals. For each radical, the most likely pathways are highlighted in black for a clearer presentation. In the three cases, the pathways with the lowest energy barriers are the β-scission pathways, and certain isomerization pathways in the cases of DEC and EMC. The migration pathways of the radical to the ether-oxygen in all cases have the highest energy barriers, followed by the migrations of the radical to the central carbon of the solvent. However, when this pathway eventually leads to the same products as for the β-scission, then it has a very close energy barrier to that of the β-scission case.

In the context of thermal runaway within a lithium-ion battery, the presently investigated reaction scheme does not directly contribute to the exothermicity of this critical process. Although the H-atom abstraction reactions are slightly exothermic, the subsequent reactions of the freshly formed radicals are all endothermic. Ultimately, the exothermicity fueling the thermal runaway comes from the formation of CO_2 and interactions with oxidizing agents.

3.2 | H-Atom Abstraction by Hydrogen and Methyl Radicals in the Gas Phase

As mentioned earlier, the H-atom abstractions by hydrogen radicals and methyl radicals are studied. All rate coefficients are provided per site, meaning they include all abstractable H-atoms situated at a specific carbon site. For the three carbonates, the abstraction by hydrogen radicals is faster than that by methyl radicals at all positions. This trend is consistent with similar abstraction reactions in the literature [44], and it agrees with the PESs, where the energy barriers are consistently lower for abstraction by Ḣ.

Three-parameter Arrhenius expressions are fitted to reaction rate constants and are presented for all abstractions in Figure 3. The comparison between the rate constants of the three different solvents' radicals for the abstraction by Ḣ shows that the fastest abstraction belongs to DEC to give the secondary carbon radical, closely followed by EMC to give the same radical position as well. This was expected, as abstraction from a secondary carbon is known to be favored over abstraction from a primary carbon. For abstraction by a methyl radical, abstraction from the secondary positions of EMC and DEC is also the fastest at the lower end of the investigated temperature regime, yet abstraction at the primary carbons starts to take over with increasing temperature due to the larger number of H-atoms at these sites. Interestingly, compared to abstraction by Ḣ, the rate coefficients for abstraction from the secondary site are not as clearly distinct from those for abstraction from the primary sites for abstraction by Ċ H_3. This is firstly due to the wider spread of activation energies among the three abstraction sites of EMC. Secondly, abstraction at the secondary site by Ċ H_3 comes with more pronounced steric hindrance compared to abstraction at the primary sites. Steric hindrance is mostly irrelevant for abstraction by Ḣ. Figure 4 shows the corresponding transition state for H-atom abstraction from the secondary site of EMC by Ċ H_3. transition state for H-atom abstraction from the secondary site of EMC by Ċ H_3.

Figure 5 shows the variation of literature rate coefficients for H-atom abstraction via Ḣ and Ċ H_3 from the three title compounds. The literature values are taken from Peukert et al. [17], Nakamura

TABLE 1 | Potential energies in kcal/mol for all energetically important stationary points of DMC, DEC, and EMC.

Stationary point	ZPE-corrected energy/kcal/mol
DMC	
RH+H	5.4
TS RH+H → R+H2	16.2
RH+CH3	4.6
TS RH+CH3 → R+CH4	18.7
R	0.0
TS R → COC(=O)C[O]	36.2
COC(=O)C[O]	13.6
TS COC(=O)C[O] → COC=O + C=O	19.4
TS R → COC=O + C=O	37.5
COC=O + C=O	24.3
DEC	
RH+H	2.6
TS RH+H → R1+H2	14.2
TS RH+H → R2+H2	11.0
RH+CH3	1.8
TS RH+CH3 → R1+CH4	16.6
TS RH+CH3 → R2+CH4	14.0
R1	0.0
TS R1 → CCOC(=O)[O] + C=C	26.4
CCOC(=O)[O] + C=C	23.7
TS R1 → R2	26.6
R2	−4.4
TS R2 → CO[C]=O + CC=O	29.6
CO[C]=O + CC=O	16.1
EMC	
RH+H	2.6
TS RH+H → R1+H2	14.3
TS RH+H → R2+H2	11.1
TS RH+H → R3+H2	13.3
RH+CH3	1.8
TS RH+CH3 → R1+CH4	16.7
TS RH+CH3 → R2+CH4	14.0
TS RH+CH3 → R3+CH4	15.9
R1	0.0
TS R1 → COC(=O)[O] + C=C	26.6
COC(=O)[O] + C=C	23.9
TS R1 → R2	41.2
TS R1 → R3	28.7
R2	−4.4
TS R2 → CO[C]=O + CC=O	30.1
CO[C]=O + CC=O	16.4
TS R2 → R3	28.9
R3	−2.8
TS R3 → CCOC(=O)C[O]	33.1
CCOC(=O)C[O]	10.7
TS CCOC(=O)C[O] → CCO[C]=O + C=O	25.9
TS R3 → CCO[C]=O + C=O	34.2
CCO[C]=O + C=O	21.1

Note: Species without specific names (such as RH) are identified via SMILES.

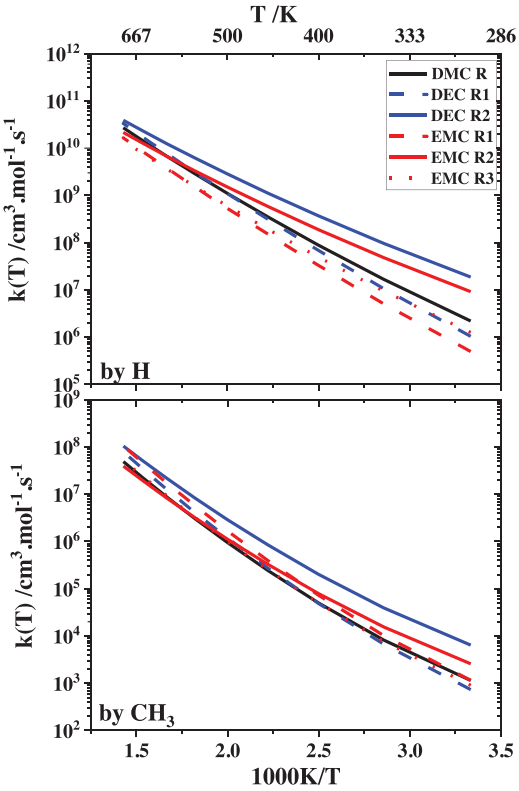

FIGURE 3 | Site-specific rate constants for hydrogen abstraction reactions by Ḣ and Ċ H_3 for DMC, DEC, and EMC.

et al. [45], and Yu et al. [46], with the latter two being either based on rate rules or analogies to DMC.

All literature rate coefficients show an increasing discrepancy from the presently calculated rates with decreasing temperature. H-atom abstraction via Ḣ and Ċ H_3 both differ by up to three orders of magnitude, with DEC and EMC showing the largest discrepancies. Interestingly, all literature rate coefficients are larger than the presently predicted rates. For DMC, the largest difference to the rate coefficient of Peukert et al. [17] amounts to almost a factor of 5. This difference can be explained by the combined differences in activation energies (10.84 kcal/mol vs.

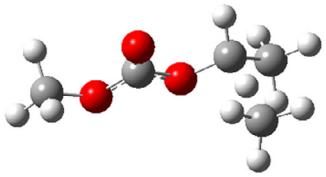

FIGURE 4 | A scheme of the hydrogen abstraction from the secondary carbon of EMC by $\dot{C}H_3$.

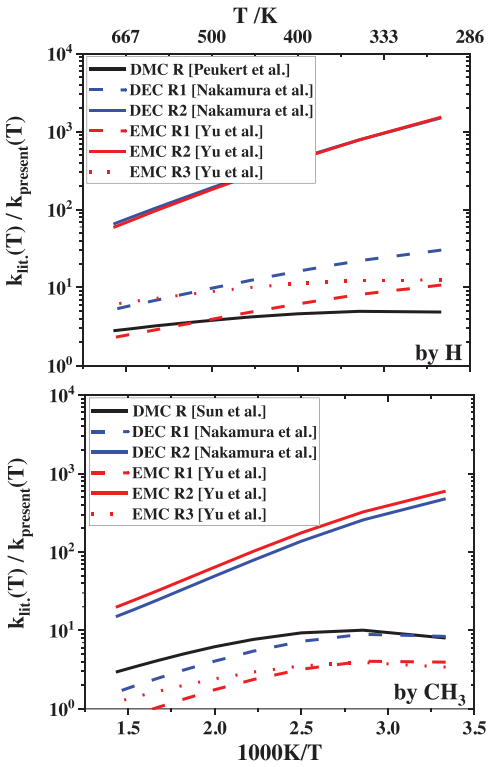

FIGURE 5 | H-atom abstraction comparison to literature.

10.49 kcal/mol [17]) and imaginary frequencies (1303 cm^{-1} vs. 1662 cm^{-1} [17]). While the difference in activation energies accounts for a factor of 1.79 at most, the difference in imaginary frequencies accounts for a factor of up to 4.03 in the tunneling correction. Given that the total tunneling correction factor is about 7 at 300 K for the present level of theory, a difference of factor 4.03 is in the same order of magnitude as the effect itself. Testing a quartic tunneling correction for DMC + $\dot{H}$ gave a total tunneling correction factor of 10 at 300 K. At 500 K, the difference between the quartic and Eckart tunneling corrections, however, dropped to 5.6%, indicating that the Eckart tunneling correction is sufficiently accurate for elevated temperatures. The imaginary frequency directly affects the prediction of tunneling coefficients, and thus becomes increasingly important with decreasing temperature. While Peukert et al. [17] used M06-2X/cc-pVTZ for the H-atom abstraction transition state optimization, B3LYP-D3BJ/def2-TZVP was used in the present work, resulting in imaginary frequencies of 1662 and 1303 cm^{-1}, respectively, for H-atom abstraction from DMC via H. As shown in the SI, the present and the Peukert et al. [17] rate coefficients agree within a factor of 2 for temperatures above 1000 K. It is known that the imaginary frequency can rather strongly scatter with the level of

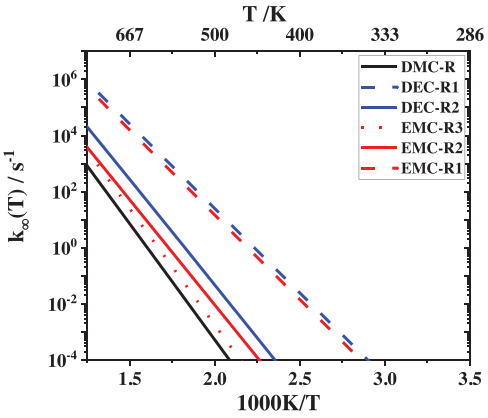

FIGURE 6 | Site-specific rate constants for thermal β-scission of radicals from different reactants.

theory [47], causing strongly pronounced uncertainties especially at low temperature conditions. There is an urgent need for future systematic investigations into imaginary frequency uncertainties of varying levels of theory.

3.3 | β-scission and Isomerization

As represented in the PESs of the dialkyl carbonates, β-scission and isomerization pathways are the most significant. A comparison between all the rates of β-scission pathways is illustrated in Figure 6.

These rates depend on the position of the radical in the molecule, as the highest rates belong to the β-scission of the primary radicals on the ethyl group of DEC and EMC, and the lowest rate corresponds to the DMC radical. On the other hand, certain radicals favor isomerization over β-scission, and the results are consistent between the PESs and the rates of these reactions presented in Figure 7. Looking at R2 of DEC, the isomerization pathway will show larger rates at lower temperatures, and as the temperature increases, the β-scission reaction dominates (crossing not shown due to very low-rate coefficients). EMC radicals R2 and R3, however, show comparable or larger rates for isomerization over the entire temperature range.

As documented in the PES of EMC in the SI, the energy barriers for the β-scission pathways are higher than the barrier of isomerization between the two radicals. Comparing the rates of this isomerization between R2 and R3, it appears that the direction of giving R2 is faster. This means that the amplified production of R3 leads to more production of R2 via isomerization, and thus indirectly to more R2 dissociation products.

3.4 | Solvation

All the calculations that are done for the reactions in the gas phase are also computed in the liquid phase using the same level of theory, but with the PCM for describing solvation. This level of theory for describing solvation is not sufficient to obtain definite liquid-phase kinetics, yet we aim at gaining first insights into how kinetics change when considering solvation effects. Here, we are

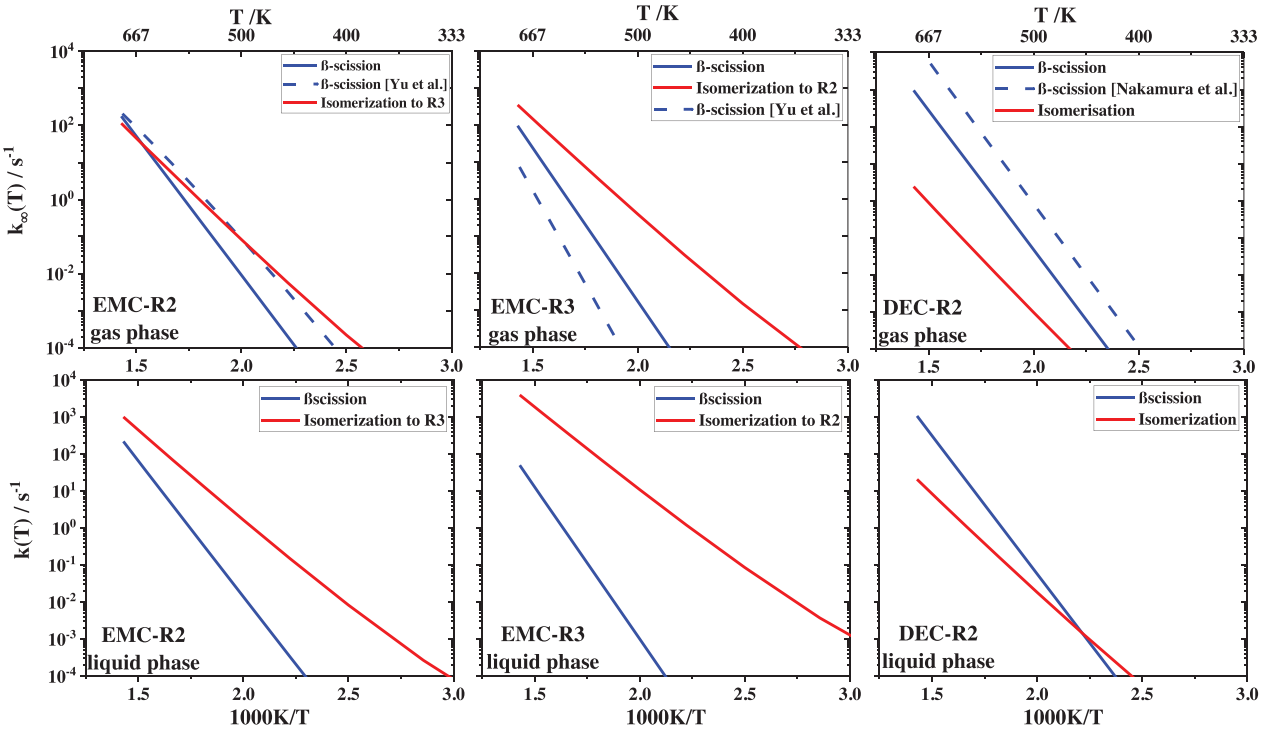

FIGURE 7 | Difference between β-scission and Isomerization pathways for DEC and EMC in gas and liquid phases.

showing only those reactions that are significantly affected by solvation effects.

3.4.1 | H-Atom Abstraction Reactions

All H-atom abstraction reactions are similarly affected by solvation, with Figure 8 showing a comparison of H-atom abstraction in the liquid and gas phases (solid and dashed lines, respectively). The use of PCM changed the activation energies for H-atom abstraction by either radical consistently. For abstraction by Ḣ, barrier heights for abstraction from both sides of the ethyl side chains of EMC and DEC are lowered by about 0.2 kcal/mol, yet barrier heights for abstraction from the methyl side chains of EMC and DMC increase by about 0.2 kcal/mol. In contrast, all barrier heights increase for the liquid phase H-atom abstraction via Ċ H_3, yet consistently shifted by about 0.5 kcal/mol relative to the solvation effects on abstraction via Ḣ.

For H-atom abstraction via Ḣ at the ethyl side chain, the barrier height dictates the change of reactivity through solvation. For both sites of the ethyl side chain, the H-atom abstraction rate coefficient is systematically larger in the liquid phase. Notably, H-atom abstraction at the methyl group of EMC is also faster in the liquid phase, contrary to the change in activation energy, which can be explained by solvation increasing the activation entropy, leading to a faster H-atom abstraction in the liquid phase. For H-atom abstraction by Ċ H_3 all rate coefficients are consistently smaller in the liquid phase compared to the gas phase, as indicated by the change in activation energy. In summary, activation energies for H-atom abstraction by Ḣ are only weakly affected by solvation, leaving space for changes in activation entropy to noticeably affect rate coefficients in the liquid phase. For H-atom abstraction by Ċ H_3, however, changes in activation energies determine how rate coefficients behave in the liquid phase compared to the gas phase.

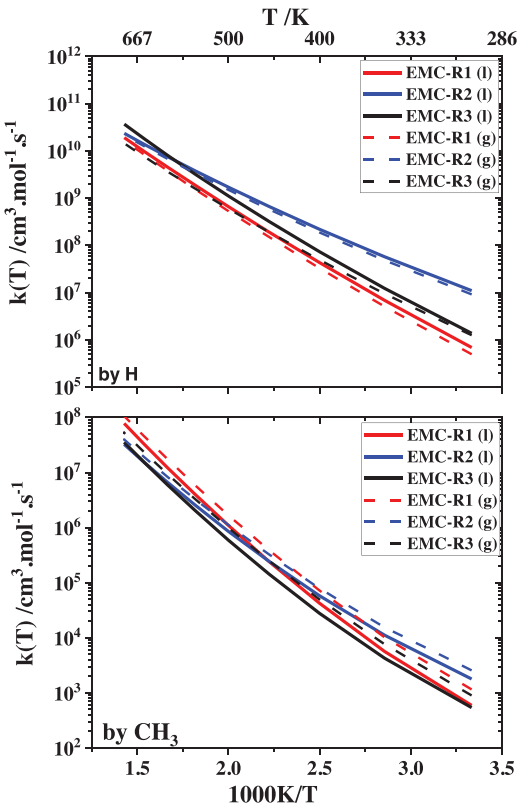

FIGURE 8 | Rate parameters for hydrogen abstraction by Ḣ and Ċ H_3 for EMC in solvation.

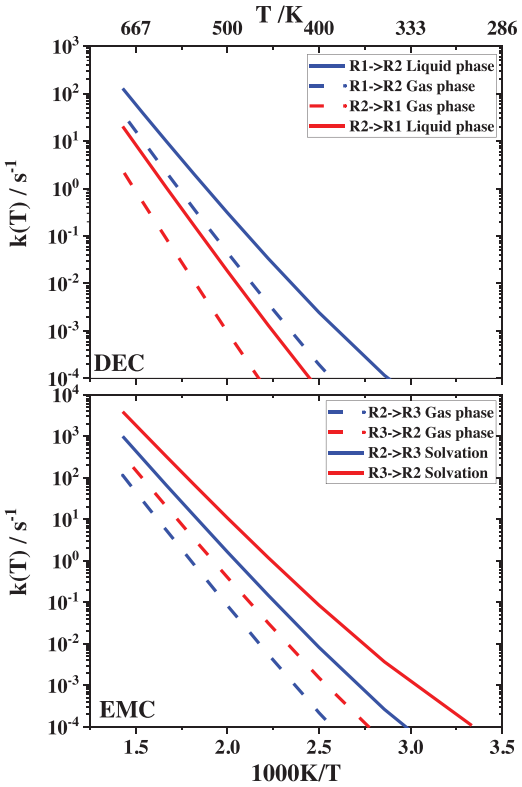

FIGURE 9 | Effect of solvation on isomerization reactions of DEC and EMC.

3.4.2 | β-Scission vs. Isomerization

The dominating reactions are the same in the gas and the liquid phases; however, the rates of the reactions are partly different. Looking at Figure 7, the crossing point between isomerization and β-scission is now at higher temperatures for all compounds shown here, meaning that isomerization is more pronounced at lower temperatures in the liquid than in the gas phase. Isomerization reactions are most affected by the solvation, which is due to the larger change in dipole moment associated with this type of reaction, compared to β-scission. As an example, the isomerization transition state between EMC-R2 and R3 comes with a dipole moment of 5.02 Debye, while the corresponding EMC-R2 β-scission transition state has a dipole moment of 2.33 Debye. As a consequence, the impact of the PCM on the activation energy is profoundly amplified for the isomerization transition state, changing it by −2.3 kcal/mol for isomerization, yet only 0.6 kcal/mol for β-scission.

In Figure 9, the rates of the dominating isomerization reactions of DEC and EMC are represented for both phases to highlight the difference. The isomerization reaction rates in the liquid phase are larger than those in the gas phase by almost two orders of magnitude at the lowest temperatures. This difference between liquid and gas phases is primarily determined through the differences in activation energies. The aforementioned change of activation energy through solvation effects of −2.3 kcal/mol causes the rate coefficient to increase by about a factor of 50 at 300 K.

4 | Conclusion

In this work, the rate parameters of H-atom abstraction reactions by Ḣ and Ċ H_3 of dimethyl-, diethyl-, and ethyl–methyl carbonates, and the subsequent radical isomerization, β-scission, and internal migration reactions were computed using B3LYP-D3BJ/def2-TZVP level of theory for the geometries and vibrational harmonic frequencies, and the CCSD(T) level of theory with augmented double- and triple-zeta basis functions (aug-cc-pV(T+D)Z) to calculate SPEs. This has been done for the gas and liquid phases.

The results show that the rate of H-atom abstraction reactions by Ḣ are always larger than those for abstractions by Ċ H_3, which is consistent with literature findings [44]. For the unimolecular radical chemistry, the β-scission and the isomerization reactions are dominating. In contrast, the energy barriers of the internal radical migration reactions are very high, except for the radical migration to the central carbon, leading to the same products as for the corresponding β-scission. The rates for β-scission reactions are larger than isomerization rates in all cases, except for the case of EMC radicals R2 and R3, and DEC radical R2 at low temperatures.

The direct comparison between the rates with and without solvation effects did not show an important change for most of the reactions using the present level of theory, namely, PCM. However, the isomerization reactions of EMC and DEC were substantially affected. It is found that the magnitude of the dipole moment of the corresponding transition states strongly determines the impact of solvation on the rate coefficients. Further research with more elaborate solvation models is advised.

With the present findings, future detailed chemical kinetic modeling studies will be enabled to predict the ignition and flame safety of the presently studied carbonates more reliably.

Acknowledgments

M.S. was funded by the ANR SFRI (21-SFRI-0005) GRAEL program of the University of Lille. The CaPPA project (Chemical and Physical Properties of the Atmosphere) is funded by the French National Research Agency (ANR) through the PIA (Programme d'Investissement d'Avenir) under contract "ANR-11-LABX-0005–01" and by the Regional Council "Hauts-de-France" and the "European Funds for Regional Economical Development" (FEDER). This work was funded by the Deutsche Forschungsgemeinschaft (DFG, German Research Foundation) – 535189852. Simulations were performed with computing resources granted by RWTH Aachen University under project RWTH0515.

Open access funding enabled and organized by Projekt DEAL.

Conflicts of Interest

The authors declare no conflicts of interest.

Data Availability Statement

The data that support the findings of this study are available within the article and its supplementary material.

References

1. M. Saab, G. Vanhove, and Y. Fenard, "On the Influence of Hydrogen on the Low-Temperature Reactivity of n-Pentane, 1-Pentene and 3-Pentanone: An Experimental and Modeling Study," *Proc. Combust. Inst.* (2022) S1540748922001730, https://doi.org/10.1016/j.proci.2022.07.145.

2. D. Petrovic, D. Pesic, M. Petrovic, and R. Mijailovic, "Electric Cars: Are They Solution to Reduce CO2 Emission?" *Thermal Science* 24 (2020): 2879–2889, https://doi.org/10.2298/TSCI191218103P.

3. A. R. Quinteros-Condoretty, S. R. Golroudbary, L. Albareda, B. Barbiellini, and A. Soyer, "Impact of Circular Design of Lithium-Ion Batteries on Supply of Lithium for Electric Cars towards a Sustainable Mobility and Energy Transition," *Procedia CIRP* 100 (2021): 73–78, https://doi.org/10.1016/j.procir.2021.05.012.

4. K. Amine, I. Belharouak, Z. Chen, et al., "Nanostructured Anode Material for High-Power Battery System in Electric Vehicles," *Advanced Materials* 22 (2010): 3052–3057, https://doi.org/10.1002/adma.201000441.

5. D. Ouyang, M. Chen, Q. Huang, J. Weng, Z. Wang, and J. Wang, "A Review on the Thermal Hazards of the Lithium-Ion Battery and the Corresponding Countermeasures," *Applied Sciences* 9 (2019): 2483, https://doi.org/10.3390/app9122483.

6. T. A. Barnes, J. W. Kaminski, O. Borodin, and T. F. Miller, "*Ab Initio* Characterization of the Electrochemical Stability and Solvation Properties of Condensed-Phase Ethylene Carbonate and Dimethyl Carbonate Mixtures," *Journal of Physical Chemistry C* 119 (2015): 3865–3880, https://doi.org/10.1021/jp510882g.

7. C. S. Cheung, R. Zhu, and Z. Huang, "Investigation on the Gaseous and Particulate Emissions of a Compression Ignition Engine Fueled With Diesel–Dimethyl Carbonate Blends," *Science of the Total Environment* 409 (2011): 523–529, https://doi.org/10.1016/j.scitotenv.2010.10.027.

8. M. Kozak, J. Merkisz, P. Bielaczyc, and A. Szczotka, "The Influence of Oxygenated Diesel Fuels on a Diesel Vehicle PM/no_x Emission Trade-Off," 2009: 2009-01-2696, https://doi.org/10.4271/2009-01-2696.

9. G. D. Zhang, H. Liu, X. X. Xia, W. G. Zhang, and J. H. Fang, "Effects of Dimethyl Carbonate Fuel Additive on Diesel Engine Performances," *Proceedings of the Institution of Mechanical Engineers, Part J: Journal of Automobile Engineering* 219 (2005): 897–903, https://doi.org/10.1243/095440705x28358.

10. A. Sinha and M. J. Thomson, "The Chemical Structures of Opposed Flow Diffusion Flames of C3 Oxygenated Hydrocarbons (Isopropanol, Dimethoxy Methane, and Dimethyl Carbonate) and Their Mixtures," *Combustion and Flame* 136 (2004): 548–556, https://doi.org/10.1016/j.combustflame.2003.12.011.

11. P. A. Glaude, W. J. Pitz, and M. J. Thomson, "Chemical Kinetic Modeling of Dimethyl Carbonate in an Opposed-Flow Diffusion Flame," *Proceedings of the Combustion Institute* 30 (2005): 1111–1118, https://doi.org/10.1016/j.proci.2004.08.096.

12. M. E. Bardin, E. V. Ivanov, E. J. K. Nilsson, V. A. Vinokurov, and A. A. Konnov, "Laminar Burning Velocities of Dimethyl Carbonate With Air," *Energy & Fuels* 27 (2013): 5513–5517, https://doi.org/10.1021/ef401108a.

13. M. Henriksen, K. Vaagseather, A. V. Gaathaug, J. Lundberg, S. Forseth, and D. Bjerketvedt, "Laminar Burning Velocity of the Dimethyl Carbonate–Air Mixture Formed by the Li-Ion Electrolyte Solvent," *Combustion, Explosion, and Shock Waves* 56 (2020): 383–393, https://doi.org/10.1134/S0010508220040024.

14. E. Hu, Y. Chen, Z. Zhang, et al., "Experimental and Kinetic Study on Ignition Delay Times of Dimethyl Carbonate at High Temperature," *Fuel* 140 (2015): 626–632, https://doi.org/10.1016/j.fuel.2014.10.013.

15. K. Alexandrino, M. U. Alzueta, and H. J. Curran, "An Experimental and Modeling Study of the Ignition of Dimethyl Carbonate in Shock Tubes and Rapid Compression Machine," *Combustion and Flame* 188 (2018): 212–226, https://doi.org/10.1016/j.combustflame.2017.10.001.

16. T. Atherley, S. de Persis, N. Chaumeix, et al., "Laminar Flame Speed and Shock-Tube Multi-Species Laser Absorption Measurements of Dimethyl Carbonate Oxidation and Pyrolysis Near 1 atm," *Proceedings of the Combustion Institute* 38 (2021): 977–985, https://doi.org/10.1016/j.proci.2020.06.333.

17. S. L. Peukert, R. Sivaramakrishnan, and J. V. Michael, "High Temperature Shock Tube and Theoretical Studies on the Thermal Decomposition of Dimethyl Carbonate and Its Bimolecular Reactions With H and D-Atoms," *Journal of Physical Chemistry A* 117 (2013): 3718–3728, https://doi.org/10.1021/jp312643k.

18. H. Nakamura, H. J. Curran, A. Polo Córdoba, et al., "An Experimental and Modeling Study of Diethyl Carbonate Oxidation," *Combustion and Flame* 162 (2015): 1395–1405, https://doi.org/10.1016/j.combustflame.2014.11.002.

19. W. Sun, C. Huang, T. Tao, et al., "Exploring the High-Temperature Kinetics of Diethyl Carbonate (DEC) Under Pyrolysis and Flame Conditions," *Combustion and Flame* 181 (2017): 71–81, https://doi.org/10.1016/j.combustflame.2017.03.009.

20. R. Shahla, C. Togbé, S. Thion, et al., "Burning Velocities and Jet-Stirred Reactor Oxidation of Diethyl Carbonate," *Proceedings of the Combustion Institute* 36 (2017): 553–560, https://doi.org/10.1016/j.proci.2016.06.041.

21. M. AlAbbad, B. R. Giri, M. Szőri, B. Viskolcz, and A. Farooq, "A High Temperature Kinetic Study for the Thermal Unimolecular Decomposition of Diethyl Carbonate," *Chemical Physics Letters* 684 (2017): 390–396, https://doi.org/10.1016/j.cplett.2017.07.020.

22. R. Notario, J. Quijano, C. Sánchez, and E. Vélez, "Theoretical Study of the Mechanism of Thermal Decomposition of Carbonate Esters in the Gas Phase," *Journal of Physical Organic Chemistry* 18 (2005): 134–141, https://doi.org/10.1002/poc.866.

23. P. Sela, Y. Zhang, J. Herzler, M. Fikri, C. Schulz, and S. Peukert, "Pyrolysis of Diethyl Carbonate: Shock-Tube and Flow-Reactor Measurements and Modeling," *Proceedings of the Combustion Institute* 38 (2021): 987–996, https://doi.org/10.1016/j.proci.2020.07.052.

24. J. Cross, R. Hunter, and V. Stimson, "The Thermal Decomposition of Simple Carbonate Esters," *Australian Journal of Chemistry* 29 (1976): 1477, https://doi.org/10.1071/CH9761477.

25. J. Herzler, J. A. Manion, and W. Tsang, "Single-Pulse Shock Tube Studies of the Decomposition of Ethoxy Compounds," *Journal of Physical Chemistry A* 101 (1997): 5494–5499, https://doi.org/10.1021/jp970653a.

26. A. S. Gordon and W. P. Norris, "A Study of the Pyrolysis of Methyl Ethyl and Diethyl Carbonates in the Gas Phase," *Journal of Physical Chemistry* 69 (1965): 3013–3017, https://doi.org/10.1021/j100893a032.

27. R. Taylor, "Abnormal Rate Spread in Pyrolysis of Alkyl Methyl Carbonates and S-Alkyl O-Methyl Carbonates due to Enhanced Nucleophilicity of the Carbonyl Group," *Journal of the Chemical Society, Perkin Transactions* 2 (1983): 291, https://doi.org/10.1039/p29830000291.

28. R. Añez, A. Herize, A. Sierraalta, T. Cordova, and G. Chuchani, "DFT Study of Substituent Effects of 2-Substituted Alkyl Ethyl Methylcarbonates in Homogeneous, Unimolecular Gas Phase Elimination Kinetics," *International Journal of Chemical Kinetics* 38 (2006): 184–193, https://doi.org/10.1002/kin.20159.

29. G. Chuchani, E. Marquez, A. Herize, R. M. Domínguez, M. Tosta, and D. Brusco, "Mechanism and Structure–Reactivity Correlation in the Homogeneous, Unimolecular Elimination Kinetics of 2-Substituted Ethyl Methylcarbonates in the Gas Phase," *Journal of Physical Organic Chemistry* 16 (2003): 839–848, https://doi.org/10.1002/poc.665.

30. K. Kanayama, S. Takahashi, S. Morikura, H. Nakamura, T. Tezuka, and K. Maruta, "Study on Oxidation and Pyrolysis of Carbonate Esters Using a Micro Flow Reactor With a Controlled Temperature Profile. Part I: Reactivities of Dimethyl Carbonate, Ethyl Methyl Carbonate and Diethyl Carbonate," *Combustion and Flame* 237 (2022): 111810, https://doi.org/10.1016/j.combustflame.2021.111810.

31. S. Takahashi, K. Kanayama, S. Morikura, H. Nakamura, T. Tezuka, and K. Maruta, "Study on Oxidation and Pyrolysis of Carbonate Esters Using a Micro Flow Reactor With a Controlled Temperature Profile. Part II: Chemical Kinetic Modeling of Ethyl Methyl Carbonate," *Combustion*

and Flame 238 (2022): 111878, https://doi.org/10.1016/j.combustflame.2021.111878.

32. C. M. Grégoire, S. P. Cooper, M. Khan-Ghauri, S. A. Alturaifi, E. L. Petersen, and O. Mathieu, "Pyrolysis Study of Dimethyl Carbonate, Diethyl Carbonate, and Ethyl Methyl Carbonate Using Shock-Tube Spectroscopic CO Measurements and Chemical Kinetics Investigation," *Combustion and Flame* 249 (2023): 112594, https://doi.org/10.1016/j.combustflame.2022.112594.

33. Gaussian 09, Revision D.01, M. J. Frisch, G. W. Trucks, H. B. Schlegel, et al., *Gaussian 09* (Gaussian, Inc., 2016). Revision D.01.

34. A. Halkier, T. Helgaker, P. Jørgensen, et al., "Basis-Set Convergence in Correlated Calculations on Ne, N_2, and H_2O," *Chemical Physics Letters* 286 (1998): 243–252, https://doi.org/10.1016/S0009-2614(98)00111-0.

35. J. Zheng, Y. Zhao, and D. G. Truhlar, "The DBH24/08 Database and Its Use to Assess Electronic Structure Model Chemistries for Chemical Reaction Barrier Heights," *Journal of Chemical Theory and Computation* 5 (2009): 808–821, https://doi.org/10.1021/ct800568m.

36. J. C. Rienstra-Kiracofe, W. D. Allen, and H. Schaefer III, "The C_2H_5 + O_2 Reaction Mechanism: High-level Ab Initio Characterizations," *Journal of Physical Chemistry A* 104 (2000): 9823–9840.

37. Y. Georgievskii, J. A. Miller, M. P. Burke, and S. J. Klippenstein, "Reformulation and Solution of the Master Equation for Multiple-Well Chemical Reactions," *Journal of Physical Chemistry A* 117 (2013): 12146–12154, https://doi.org/10.1021/jp4060704.

38. H.-H. Carstensen and A. M. Dean, "Chapter 4 the Kinetics of Pressure-Dependent Reactions," *Comprehensive Chemical Kinetics* (2007): 101–184, https://doi.org/10.1016/S0069-8040(07)42004-0.

39. M. Döntgen, M. E. Fuller, S. Peukert, et al., "Shock Tube Study of the Pyrolysis Kinetics of Di- and Trimethoxy Methane," *Combustion and Flame* 242 (2022): 112186, https://doi.org/10.1016/j.combustflame.2022.112186.

40. H. Hippler, J. Troe, and H. J. Wendelken, "Collisional Deactivation of Vibrationally Highly Excited Polyatomic Molecules. II. Direct Observations for Excited Toluene," *Journal of Chemical Physics* 78 (1983): 6709–6717, https://doi.org/10.1063/1.444670.

41. J. Self, N. T. Hahn, and K. A. Persson, "Solvation Effects on the Dielectric Constant of 1 M LiPF6 in Ethylene Carbonate: Ethyl Methyl Carbonate 3:7," *Energy & Environmental Materials* (2023) e12494, https://doi.org/10.1002/eem2.12494.

42. M. Bursch, J.-M. Mewes, A. Hansen, and S. Grimme, "Best-Practive DFT Protocols for Basic Molecular Computational Chemistry," *Angewandte Chemie International Edition* 61 (2022): e202205735.

43. M. Döntgen, L. C. Kröger, and K. Leonhard, "Hot β-Scission of Radicals Formed via Hydrogen Abstraction," *Proceedings of the Combustion Institute* 36 (2017): 135ß142.

44. L. C. Kröger, M. Döntgen, D. Firaha, W. A. Kopp, and K. Leonhard, "Ab Initio Kinetics Predictions for H-Atom Abstraction From Diethoxymethane by Hydrogen, Methyl, and Ethyl Radicals and the Subsequent Unimolecular Reactions," *Proceedings of the Combustion Institute* 37 (2019): 275–282, https://doi.org/10.1016/j.proci.2018.06.056.

45. H. Nakamura, H. J. Curran, A. Polo Córdoba, et al., "An Experimental and Modeling Study of Diethyl Carbonate Oxidation," *Combustion and Flame* 162 (2015): 1395–1405, https://doi.org/10.1016/j.combustflame.2014.11.002.

46. R. Yu, J. Liu, Y. Wu, and C. Tang, "Experimental and Modeling Study on Ignition Kinetics of Ethyl Methyl Carbonate," *Combustion and Flame* 261 (2024): 113318, https://doi.org/10.1016/j.combustflame.2024.113318.

47. J. Elm, S. Jørgensen, M. Bilde, and K. V. Mikkelsen, "Ambient Reaction Kinetics of Atmospheric Oxygenated Organics With the OH Radical: A Computational Methodology Study," *Physical Chemistry Chemical Physics* 15 (2013): 9636, https://doi.org/10.1039/c3cp50192b.

Supporting Information

Additional supporting information can be found online in the Supporting Information section.

Supplementary File 1: kin70007-sup-0001-SuppMat.pdf. **Supplementary File 2**: kin70007-sup-0002-SuppMat.zip.